ELSEVIER

Nuclear Instruments and Methods in Physics Research B 146 (1998) 19–28

NIM B
Beam Interactions with Materials & Atoms

Resonant coherent excitation of 390 MeV/u Ar ions planar channeled in Si crystals

K. Komaki [a,*], T. Azuma [a], T. Ito [a], Y. Takabayashi [a], Y. Yamazaki [a], M. Sano [b], M. Torikoshi [b], A. Kitagawa [b], E. Takada [b], T. Murakami [b]

[a] *Institute of Physics, Graduate School of Arts and Sciences, University of Tokyo, 3-8-1 Komaba, Meguro, Tokyo 153-8902, Japan*
[b] *National Institute of Radiological Sciences, 4-9-1 Anagawa, Inage, Chiba 263-8555, Japan*

Abstract

Resonant coherent excitation of the 1s electron to $n=2$ states in a hydrogen-like ion was studied through measurements of the survived fraction of 390 MeV/u Ar^{17+} planar channeled in a Si crystal. Adopting a totally depleted Si surface barrier detector as a target crystal, the charge state of the individual emerged ion was measured in coincidence with the energy deposition in the target. By changing the incident direction along the $(2\,\bar{2}\,0)$, $(0\,0\,4)$, and $(1\,\bar{1}\,1)$ planes, a series of clear resonances were observed as the decrease in the survived charge fraction due to higher electron loss probability for the excited state. Each resonance profile reflects energy splitting of the $n=2$ manifold originated from l–s interaction and Stark effect due to the crystal field. From the correlation between the energy loss and survived charge fraction, transition energy as a function of the ion trajectory amplitude is deduced which is in good agreement with calculated results.

PACS: 61.85.+p; 34.50.Fa; 34.50.Bw; 71.70.Ej
Keywords: Resonant coherent excitation; Channeling; Electron loss process of atoms; Stopping power; Spin–orbit interaction; Stark effect

1. Introduction

An ion passing through a crystal with a constant velocity, v, feels a Fourier component of the crystal potential, $\phi_g \exp(-2\pi i \boldsymbol{g}\cdot\boldsymbol{r}')$, corresponding to a reciprocal lattice vector, $\boldsymbol{g}$, as an oscillating perturbation with a frequency, $\upsilon = \gamma \boldsymbol{g}\cdot\boldsymbol{v}$, where $\gamma = 1/\sqrt{1-\beta^2}$, $\beta = v/c$, and $\boldsymbol{r}'$ is the position vector of the ion in the rest frame of the crystal (L-frame). If the ion is channeled along a low indexed axis or plane, a set of Fourier components have a common frequency and thus exert a coherent perturbation on the ion. When this frequency satisfies a condition, $\Delta E = h\nu$, ΔE being the transition energy to an excited state in the internal degree of freedom, resonant coherent excitation (RCE) takes place.

The RCE process and the possibility of radiative deexcitation was first predicted by Okorokov [1]. The first observation of RCE was made

* Corresponding author. Tel.: 81 3 5454 6514; fax: 81 3 5454 6998; e-mail: komaki@phys.c.u-tokyo.ac.jp

0168-583X/98/$ – see front matter
PII: S0168-583X(98)00428-5

through subsequent charge stripping due to higher electron loss probability for excited states [2]. Detection of RCE through radiative deexcitation was achieved in the case of heavier ions which have smaller orbital radii of the excited electrons [3].

During last two decades, much progress in understanding the nature of RCE has been made [4]. The continuum potential of the crystal and the wake potential induced by the ion exert a stationary perturbation on the ion and give rise to a removal of the degeneracy in excited states. Each Stark-split state has a characteristic shape of the electron cloud. The strengths of the Stark field and the oscillating perturbation and the probability of the electron loss process are all dependent on the ion position in the crystal channel, the information of which is reflected on the energy loss of the ion. The channeling ion is in such a peculiar environment and RCE is an excellent probe to study the atomic processes experienced by ions in such conditions.

Observations of RCE so far have been limited to relatively light ions and to relatively low ion energies. In the present, we report the first observation of RCE of the 1s electron to $n=2$ states in Ar^{17+} through measurements of a survived fraction of Ar^{17+} planar channeled in Si crystals in the relativistic ion energy region [5]. Argon is the heaviest ion with the largest excitation energy to be observed among ever reported experiments on RCE. The effects of special relativity can be seen in the present case in several aspects. The resonance condition is significantly altered through Lorentz contraction of the crystal lattice and the orbital velocity of the bound electron is so high that the Stark mixing due to the continuum potential is strongly affected by the l–s interaction.

At high ion energies, where the electrostatic accelerators are not available, searching the resonance by altering the projectile velocity is not practical and, instead, altering the incident direction along a channeling plane is much more advantageous.

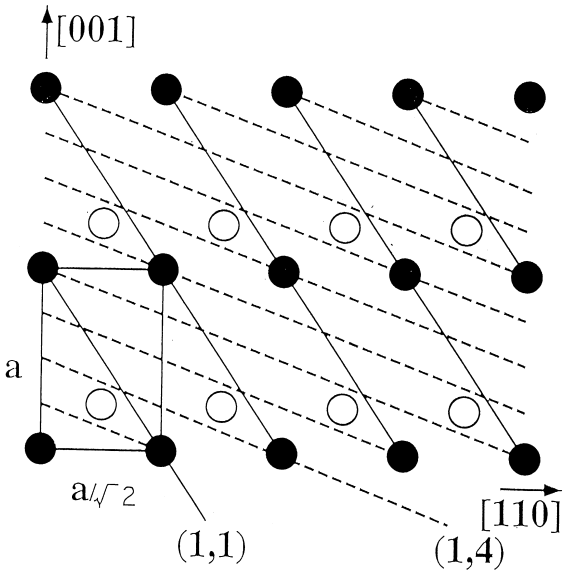

Fig. 1. Atomic arrangement on a $(2\,\bar{2}\,0)$ plane of diamond structure. 2D base vectors are $\boldsymbol{A}=[1\,1\,0]a/2$ and $\boldsymbol{B}=[0\,0\,1]a$. The solid and broken lines represent $(1,1)$ and $(1,4)$ strings, respectively.

2. Theoretical considerations

2.1. Identification of planar RCE

The frequency of the oscillating potential felt by a planar channeled ion can be understood as the frequency with which the ion passes a 'string of strings' which forms the atomic net plane. Thus the planar resonance can be identified by specifying the atomic string lying in the channeling plane. Regarding the atomic plane as a two-dimensional (2D) crystal of which unit cell is defined by two lattice vectors, $\boldsymbol{A}$ and $\boldsymbol{B}$, a set of atomic strings in this 2D lattice can be identified by a 2D Miller index, (k,l), similarly defined as in the case of a three-dimensional (3D) lattice, i.e., the direction of the (k,l) strings is parallel to a line which intersects with two axes at $\boldsymbol{A}/k$ and $\boldsymbol{B}/l$.

In the present paper, we examine three kinds of channeling planes in the diamond structure, $(2\,\bar{2}\,0)$, $(1\,\bar{1}\,1)$ and $(0\,0\,4)$, which intersect each other at $[1\,1\,0]$ axis. Fig. 1 shows the atomic arrangement on a $(2\,\bar{2}\,0)$ plane, where the 2D base vectors are $\boldsymbol{A}=[1\,1\,0]a/2$ and $\boldsymbol{B}=[0\,0\,1]a$, where a is the lattice constant. The solid and broken lines in the figure represent $(1,1)$ and $(1,4)$ strings, respectively. For $(1\,\bar{1}\,1)$ and $(0\,0\,4)$ planes, 2D base

vectors are chosen as $\boldsymbol{A} = [1\ 1\ 0]a/2$, $\boldsymbol{B} = [\bar{1}\ 1\ 2]a/2$ and $\boldsymbol{A} = [1\ 1\ 0]a/2$, $\boldsymbol{B} = [\bar{1}\ 1\ 0]a/2$, respectively.

2.2. RCE conditions for planar channeling

Taking a lattice vector, $\boldsymbol{C}$, to a lattice point on the neighboring atomic plane as the third base vector, a new 3D unit cell can be defined. The base vectors of the new reciprocal lattice can also be defined as $\boldsymbol{A}^*$, $\boldsymbol{B}^*$ and $\boldsymbol{C}^*$, so that $\boldsymbol{A}^*\cdot\boldsymbol{A} = \boldsymbol{B}^*\cdot\boldsymbol{B} = \boldsymbol{C}^*\cdot\boldsymbol{C} = 1$ and $\boldsymbol{A}^*\cdot\boldsymbol{B} = \boldsymbol{B}^*\cdot\boldsymbol{C} = \boldsymbol{C}^*\cdot\boldsymbol{A} = \boldsymbol{A}^*\cdot\boldsymbol{C} = \boldsymbol{B}^*\cdot\boldsymbol{A} = \boldsymbol{C}^*\cdot\boldsymbol{B} = 0$. It is to be noted that the vector $\boldsymbol{C}^*$ is identical with the reciprocal lattice vector $\boldsymbol{h}$ which denotes the channeling plane. Then a 3D reciprocal lattice vector can be represented by

$$\boldsymbol{g} = \boldsymbol{G}(k,l) + n\boldsymbol{h} = k\boldsymbol{A}^* + l\boldsymbol{B}^* + n\boldsymbol{h}. \tag{1}$$

Taking the z-axis parallel to the ion velocity and x-axis normal to the channeling plane, the ion position in the L-frame can be given as

$$\boldsymbol{R}(t') = \boldsymbol{R}_\perp + \boldsymbol{v}t' = (X, Y, vt'). \tag{2}$$

Taking note that $\boldsymbol{h}\cdot\boldsymbol{v} = 0$, the scalar potential at the ion position in L-frame is then given by

$$\begin{aligned}\phi'(\boldsymbol{R}_\perp + \boldsymbol{v}t') &= \sum_{\boldsymbol{g}} \phi_{\boldsymbol{g}} \exp[-2\pi i\boldsymbol{g}\cdot(\boldsymbol{R}_\perp + \boldsymbol{v}t')] \\ &= \sum_{kl}\sum_{n} \phi_{\boldsymbol{G}(k,l)+n\boldsymbol{h}} \\ &\quad\times \exp[-2\pi i(\boldsymbol{G}(k,l) + n\boldsymbol{h})\cdot(\boldsymbol{R}_\perp + \boldsymbol{v}t')] \\ &= \sum_{kl} \phi_{kl}(X) \exp(-2\pi i\boldsymbol{G}_\perp(k,l)\cdot\boldsymbol{R}_\perp) \\ &\quad\times \exp(-2\pi i\boldsymbol{G}(k,l)\cdot\boldsymbol{v}t'),\end{aligned} \tag{3}$$

where

$$\phi_{kl}(X) = \sum_n \phi_{\boldsymbol{G}(k,l)+n\boldsymbol{h}} \exp(-2\pi i n X/d_p) \tag{4}$$

is the amplitude of the oscillating potential due to the (k,l) string and $d_p = 1/|\boldsymbol{h}|$ is the inter planar spacing. Note that the Fourier component with $k = l = 0$,

$$\phi_{00}(x) = \sum_n \phi_{n\boldsymbol{h}} \exp(-2\pi i n x/d_p) \tag{5}$$

is independent of time and is the planar continuum potential.

If the ion velocity, $\boldsymbol{v}$, makes angles θ and $\theta' = \Theta - \theta$ with 2D base vectors, $\boldsymbol{A}$ and $\boldsymbol{B}$, Θ being the angle between $\boldsymbol{A}$ and $\boldsymbol{B}$, the velocity vector can be written as,

$$\boldsymbol{v} = (v/\sin\Theta)[\boldsymbol{A}\sin(\Theta - \theta)/A + \boldsymbol{B}\sin\theta/B] \tag{6}$$

and the L-frame frequency for the ion to pass two adjacent strings is given by

$$\begin{aligned}\nu'(k,l) &= \boldsymbol{G}(k,l)\cdot\boldsymbol{v} = (k\boldsymbol{A}^* + l\boldsymbol{B}^*)\cdot(v/\sin\Theta) \\ &\quad[\boldsymbol{A}\sin(\Theta - \theta)/A + \boldsymbol{B}\sin\theta/B] = (v/\sin\Theta) \\ &\quad[k\sin(\Theta - \theta)/A + l\sin\theta/B].\end{aligned} \tag{7}$$

As the frequency is transformed to the rest frame of the projectile (P-frame) as $\nu(k,l) = \gamma\nu'(k,l) = \gamma\boldsymbol{G}(k,l)\cdot\boldsymbol{v}$, the condition for the (k,l)-resonance is given by

$$\begin{aligned}\Delta E &= h\nu(k,l) \\ &= (\gamma h v/\sin\Theta)[k\sin(\Theta - \theta)/A + l\sin\theta/B].\end{aligned} \tag{8}$$

When $\boldsymbol{A}$ and $\boldsymbol{B}$ can be chosen perpendicular to each other, the resonance condition is simply given by,

$$\Delta E = h\nu(k,l) = \gamma h v[k\cos\theta/A + l\sin\theta/B]. \tag{9}$$

In the case of $(2\ \bar{2}\ 0)$, $(1\ \bar{1}\ 1)$ and $(0\ 0\ 4)$ planes in the diamond structure, (A,B) are $(a/\sqrt{2}, a)$, $(a/\sqrt{2}, \sqrt{\frac{3}{2}}a)$ and $(a/\sqrt{2}, a/\sqrt{2})$ respectively.

2.3. Hamiltonian for the bound electron

The Hamiltonian in P-frame of an electron bound to the projectile ion can be written as

$$H(\boldsymbol{r},t) = H_0(\boldsymbol{r}) + H_1(\boldsymbol{r}) + H_2(\boldsymbol{r}) + H_3(\boldsymbol{r},t), \tag{10}$$

where H_0 is the hydrogenic Hamiltonian, H_1 and H_2 are the stationary perturbations due to the dynamic wake field and the crystal continuum potential, respectively, and $H_3(t)$ the time-dependent perturbation due to the crystal periodic potential. For such a heavy ion as argon, where $\alpha Z_1 = Z_1/137 \ll 1$ dose not hold, the relativistic Hamiltonian has to be adopted as the unperturbed Hamiltonian,

$$H_0(r) = -c\boldsymbol{\alpha}\cdot\boldsymbol{p} - \beta mc^2 + V(r), \quad V(r) = -Z_1e^2/r, \tag{11}$$

where $\boldsymbol{\alpha}$ and β are the Dirac matrices.

The scalar potential, $\phi'(\boldsymbol{r}')$, of the crystal in the L-frame is transformed to a four-potential in the P-frame as, $A_x(\boldsymbol{r},t) = A_y(\boldsymbol{r},t) = 0$, $A_z(\boldsymbol{r},t) = -(v/c)\gamma\phi'(\boldsymbol{r}')$ and $\phi(\boldsymbol{r},t) = \gamma\phi'(\boldsymbol{r}')$. As the wake potential, $\phi_w(\boldsymbol{r})$, is stationary with respect to the projectile, the total Hamiltonian in the P-frame is given by

$$\begin{aligned} H(\boldsymbol{r},t) &= -\boldsymbol{\alpha}\cdot[c\boldsymbol{p} + e\boldsymbol{A}(\boldsymbol{r},t)] - \beta mc^2 + V(r) \\ &\quad - e[\phi_w(\boldsymbol{r}) + \phi(\boldsymbol{r},t)] \\ &= -c\boldsymbol{\alpha}\cdot\boldsymbol{p} - \beta mc^2 + V(r) \\ &\quad - e\phi_w(\boldsymbol{r}) - e\gamma\left(1 - \frac{v}{c}\alpha_z\right)\phi'(\boldsymbol{r}'). \end{aligned} \tag{12}$$

Transforming the position of the electron as $\boldsymbol{r}' = \boldsymbol{R}_\perp + \boldsymbol{r}_\perp + \gamma(z\boldsymbol{e}_z + \boldsymbol{v}t)$ and $t' = \gamma(t + vz/c^2)$ and expanding the crystal potential, $\phi'(\boldsymbol{r}')$, into string contributions, the perturbation Hamiltonians are represented by

$$H_1(\boldsymbol{r}) = -e\phi_w(\boldsymbol{r}), \tag{13}$$

$$H_2(x) = -e\gamma\left(1 - \frac{v}{c}\alpha_z\right)\phi_{00}(x), \tag{14}$$

$$\begin{aligned} H_3(r,t) = &-e\gamma\left(1 - \frac{v}{c}\alpha_z\right)\sum{}'_{kl}\phi_{kl}(X+x) \\ &\times \exp[-2\pi i\boldsymbol{G}(k,l)\cdot(\boldsymbol{R}_\perp + \boldsymbol{r}_\perp + \gamma z\boldsymbol{e}_z)] \\ &\times \exp[-2\pi i\nu(k,l)t], \end{aligned} \tag{15}$$

where $\boldsymbol{e}_z = \boldsymbol{v}/v$ is a unit vector along z-axis and the summation $\sum'_{kl}$ runs over every combination of (k,l) except for $k = l = 0$.

2.4. Stark split states

We denote the unperturbed wave function as $|n\mathrm{L}J\mu\rangle$, where n is the principal quantum number, $\mathrm{L} = s$, p the orbital angular momentum, J and μ the total angular momentum and its projection, respectively. First we calculated the eigenstates for stationary Hamiltonian, $H_{st} = H_0 + H_1 + H_2$. In the present calculation, mixing between states with different n was neglected. Then the ground state wave function remains unchanged as $|1s(1/2)\mu\rangle$ and the perturbed energy eigenvalue is given by $E_0 = E(1s) + \langle 1s(1/2)\mu|H_1(\boldsymbol{r}) + H_2(x)|1s(1/2)\mu\rangle$.

Eigenfunctions of the $n = 2$ sublevels are represented by linear combinations of those of unperturbed $n = 2$ sublevels. To obtain the wave functions and the energy eigenvalue, a secular equation,

$$\det|\langle 2\mathrm{L}J\mu|H_0(\boldsymbol{r}) + H_1(\boldsymbol{r}) + H_2(x) - E|2\mathrm{L}'J'\mu'\rangle| = 0 \tag{16}$$

was solved. In the calculation of the matrix elements of $H_1(\boldsymbol{r})$ and $H_2(x)$, linear combinations of the non-relativistic wave functions, $\mathrm{R}_{nl}(r)\mathrm{Y}_{lm}(\theta,\phi)$, with spin state, $|\uparrow\rangle$ or $|\downarrow\rangle$, were adopted as the unperturbed wave functions and contributions from minor component (positrons) are neglected. Then H_2 is approximated as $H_2(x) = -e\gamma\phi_{00}(x)$. The wake potential, $\phi_w(\boldsymbol{r})$, was calculated from a dielectric function in the plasmon pole approximation.

Fig. 2 shows the calculated shift in transition energies between perturbed $n = 1$ and $n = 2$ states of Ar^{17+} ion with respect to that in vacuum, as functions of the ion position in the $(2\,\bar{2}\,0)$ planar channel of Si. Horizontal lines are the transition energies in vacuum for $J = 1/2$ and 3/2 levels. Fig. 3 shows the composition of the wave functions for

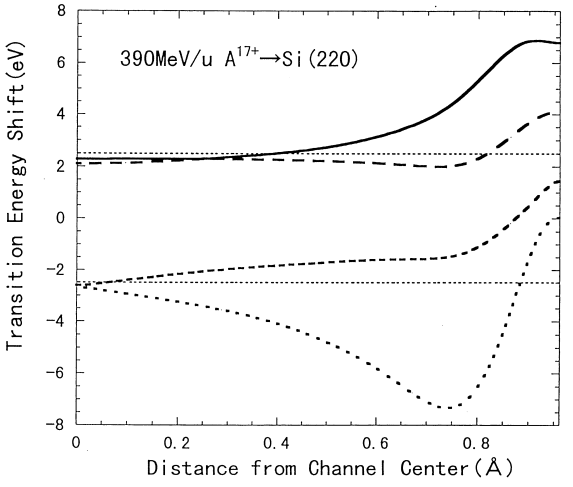

Fig. 2. Shift in transition energies between perturbed $n = 1$ and $n = 2$ substates of Ar^{17+} ion relative to that in vacuum as functions of the ion position in the $(2\,\bar{2}\,0)$ planar channel of Si. Horizontal lines are the transition energies in vacuum for $J =$ 1/2 and 3/2 levels.

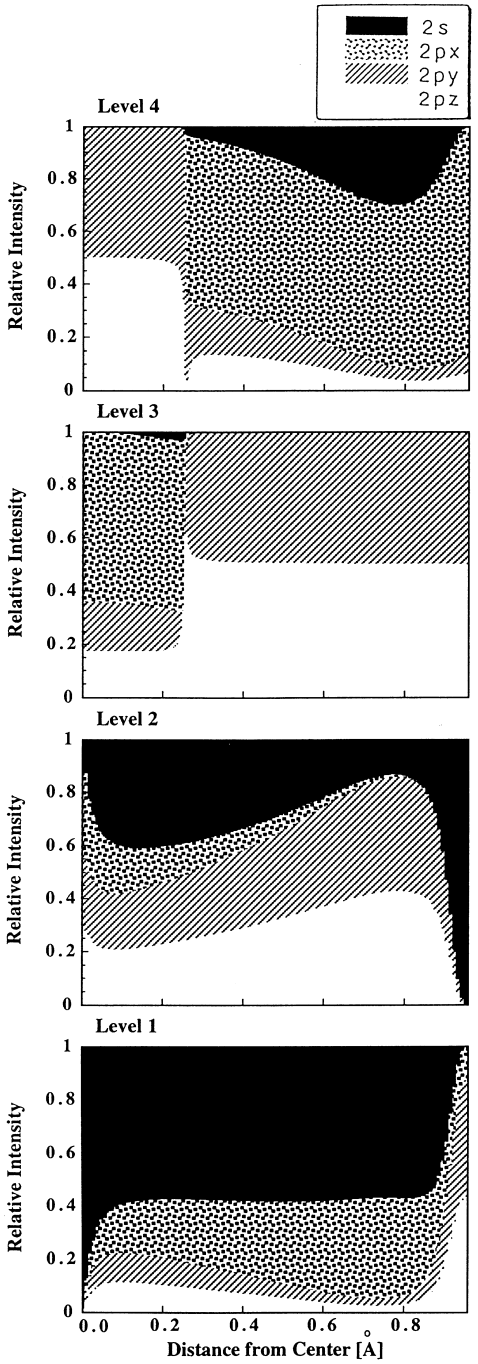

Fig. 3. Composition of the wave functions for Stark mixed $n=2$ substates of Ar^{17+} ions as functions of the ion position in the $(2\,\bar{2}\,0)$ planar channel of Si.

Stark mixed $n=2$ substates as functions of the ion position. Levels are labeled in the order of increasing level energy. Level splitting near the channel center is primarily due to the *l–s* interaction and as the ion approaches the channel wall the crystal field plays a major role resulting in the intermixing between 2s and $2p_x$ states to form $2s2p_x$(w) and $2s2p_x$(c) states as level 1 and level 4, respectively. Here (w) and (c) represent that the electron cloud is shifted towards the channel wall and center, respectively. Unlike the cases in relatively low velocities, the effect of the wake potential is negligible and as a consequence, the projection of the total angular momentum to *x*-axis (normal to the plane) is almost a good quantum number. Thus $\mu_x = \pm(3/2)$ states, which are evenly contributed by the $2p_y$ and $2p_z$ states remain pure as the level 4 at the channel center and as level 3 at the channel wall.

2.5. Transition amplitude

As described above, the energy eigenvalues and the wave functions for the stationary part of the Hamiltonian are obtained as E_j and Ψ_j, where $j=0$ denotes the ground state and $j=1$, 2, 3 and 4 the $n=2$ substates.

Time evolution of the wave function $\Psi(\boldsymbol{r},t)$ is governed by

$$\mathrm{i}(h/2\pi)\partial\Psi(\boldsymbol{r},t)/\partial t = [H_{\mathrm{st}}(\boldsymbol{r}) + H_3(\boldsymbol{r},t)]\Psi(\boldsymbol{r},t). \quad (17)$$

Expanding the wave function by those of the stationary part of the Hamiltonian,

$$\Psi(\boldsymbol{r},t) = \sum_j C_j(t)\Psi_j(\boldsymbol{r})\exp(-2\pi\mathrm{i}E_j t/h), \quad (18)$$

we get

$$\begin{aligned}
&\mathrm{i}(h/2\pi)\mathrm{d}C_j(t)/\mathrm{d}t \\
&= \sum_{j'}\langle j|H_3(\boldsymbol{r},t)|j'\rangle C_{j'}(t)\exp[2\pi\mathrm{i}(E_j - E_{j'})t/h] \\
&= -e\gamma\sum_{j'}\sum_{kl}{}'\langle j|\phi_{kl}(X+x) \\
&\quad\times\exp[-2\pi\mathrm{i}\boldsymbol{G}(k,l)\cdot(\boldsymbol{r}_\perp + \gamma z\boldsymbol{e}_z)]|j'\rangle C_{j'}(t) \\
&\quad\times\exp[-2\pi\mathrm{i}\boldsymbol{G}(k,l)\cdot\boldsymbol{R}_\perp] \\
&\quad\times\exp[2\pi\mathrm{i}\{(E_j - E_{j'})/h - v(k,l)\}t]. \quad (19)
\end{aligned}$$

Only when the RCE condition, $\Delta E_{jj'} = E_j - E_{j'} = hv(k,l)$, is satisfied, the term in the right-hand side of Eq. (19) makes a significant contribution.

It is worth noting that the factor containing the ion position, $\boldsymbol{R}_\perp$, here merely affects the phase of the wave function, but when the wave function of the ion motion is taken into account, it gives the momentum change of the ion due to RCE and consequently the energy transfer between translational and electronic degrees of freedom.

The strength of the RCE transition is then given by the matrix element,

$$M_{j0} = -e\gamma\langle j|\phi_{kl}(X+x)\exp[-2\pi i\boldsymbol{G}(k,l)\cdot(\boldsymbol{r}_\perp+\gamma z\boldsymbol{e}_z)]|0\rangle. \quad (20)$$

Fig. 4 shows the amplitudes of the perturbation potentials, $\phi_{kl}(X)$, for $(k,l)=(1,1)$, $(1,2)$, $(1,3)$, $(1,5)$ and $(1,6)$ as functions of the ion position.

3. Experimental setup

Fig. 5 illustrates top and side views of the experimental setup. A beam of hydrogen-like Ar^{17+} ions was accelerated to 390 MeV/u by Heavy Ion Medical Accelerator at Chiba (HIMAC). A parallel beam was provided by a combination of a doublet and a triplet quadruple-magnetic lenses, and was collimated by a 5 cm thick iron collimator with the inner diameter of 1 mm [6].

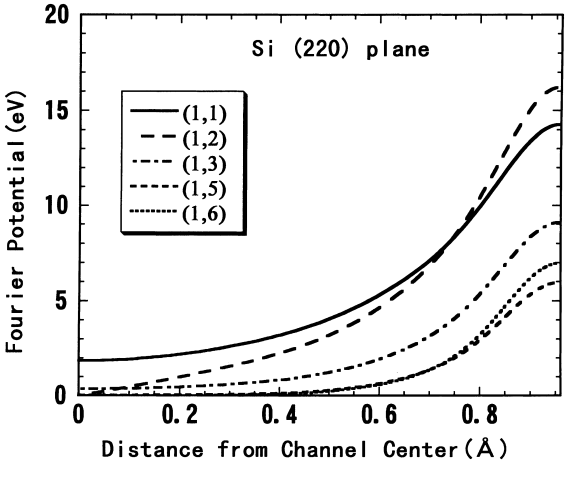

Fig. 4. Fourier potentials, ϕ_{kl}, for $(k,l)=(1,1)$, $(1,2)$, $(1,3)$, $(1,5)$ and $(1,6)$ strings in the $(2\,\bar{2}\,0)$ plane.

We used totally depleted Si surface barrier detectors of 78.5 and 94.7 μm in thickness as target crystals and at the same time as detectors for energy deposition in them, which technique has been developed in a preceding work [7]. The crystal orientation was examined by X-ray diffraction in advance and was mounted on a high-precision goniometer capable of rotating about three axes remotely and of translating along two directions normal to the beam direction.

Ions transmitted through the target were charge separated by a magnet of 0.5 T located at 1.3 m downstream of the target and were detected with a 2D-position sensitive Si detector (2D-PSD) located at 4.3 m further downstream of the magnet. A vertical slit of 1mm in width was placed at 0.6 m downstream of the target to avoid overlapping of scattered ions with different charge states. The angular divergence of the incident beam was estimated to be less than 0.15 mrad from the spot size on the 2D-PSD.

Signals from the target detector and the 2D-PSD were recorded event by event. The synchrotron was operated in a pulse mode with a repetition period of 3.3 s and the pulse width of 1.5 s. The beam intensity was reduced to a few thousand counts per second to avoid pileup.

4. Results and discussions

4.1. RCE conditions

The survived fraction of Ar^{17+} ions passing through the present Si crystal of ca. 100 μm thickness in the random direction was less than 1×10^{-3}. Under the channeling condition, however, we observed several tens percent of emerged Ar^{17+} ions. Varying the incident angle from the [1 1 0] axis in the $(2\,\bar{2}\,0)$ plane, the survived Ar^{17+} fraction was monitored. As can be seen in Fig. 6, a series of sharp decreases in the survived Ar^{17+} fraction are observed. These dips are identified as

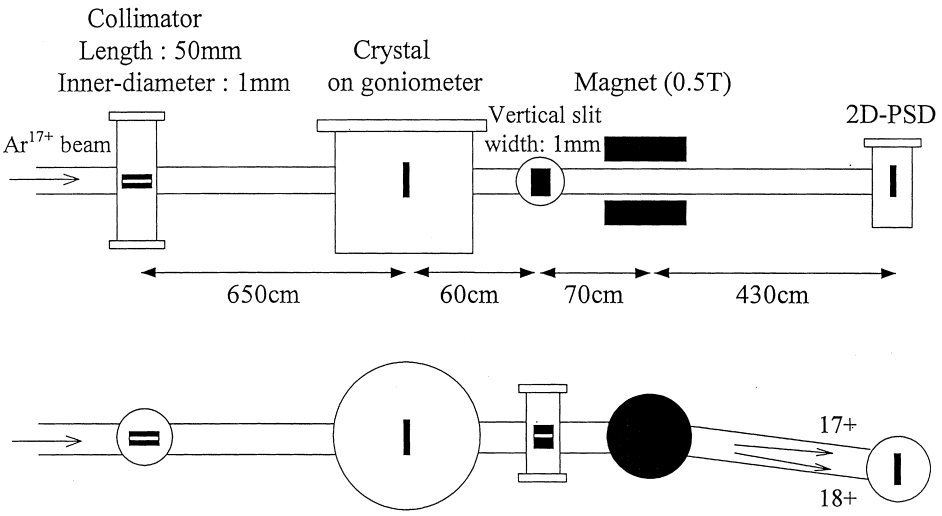

Fig. 5. Top and side views of the experimental setup.

$(k, l) = (1, 1)$, $(1, 2)$, $(1, 3)$, $(1, 5)$ and $(1, 6)$ resonances for the electronic transition from 1s to $n = 2$ states in hydrogen-like Ar ions. We changed the tilt angle, θ, also in the $(0\,0\,4)$ and $(1\,\bar{1}\,1)$ planes. As also shown in Fig. 6, resonances corresponding to $(k, l) = (1, 1)$, $(1, 2)$, $(1, 3)$, $(1, 4)$ and $(1, 5)$ for the $(0\,0\,4)$ plane and those to $(k, l) = (1, 1)$, $(1, 3)$ and $(1, 5)$ for the $(1\,\bar{1}\,1)$ plane were observed.

It is noticed that there exists a selection rule, which governs whether the (k,l) resonance should appear or not, specific to the channeling plane and to the crystal structure. The extinction of the resonance occurs when the 2D unit cell is not a primitive cell, i.e., the unit cell contains plural, equivalent atoms. In the case of $(2\,\bar{2}\,0)$ plane in the diamond structure, as seen in Fig. 1, a unit cell contains two atoms at $0\boldsymbol{A} + 0\boldsymbol{B}$ (closed circles) and $(1/2)\boldsymbol{A} + (1/4)\boldsymbol{B}$ (open circles). While the former atom is always on the (k,l) string, the latter atom lies right in the middle of two strings when $2k + l = 4n + 2$, resulting in a completely destructive interference. In the case of $(1\,\bar{1}\,1)$ plane in cubic crystals, if the 2D cell is chosen as a rectangle with a side ratio of $1 : \sqrt{3}$, (k,l) resonances with $k + l = 2n + 1$ should be absent.

The relative strength of the observed resonances for the $(2\,\bar{2}\,0)$ plane can be well explained by the calculated Fourier potential, ϕ_{kl}, shown in Fig. 4, i.e., $(1,1)$ and $(1,2)$ resonance strengths are nearly the same and $(1,6)$ resonance is even stronger than $(1,5)$ resonance. Absence of the $(1,4)$ resonance is the result of destructive interference described above.

4.2. Fine structure of the resonance

Regardless of the channeling plane, each observed resonance dip is split into several lines. Fig. 7 shows a detailed angular scan of the $(1,1)$ resonance for the $(2\,\bar{2}\,0)$ plane. For a given resonance, a given tilt angle can be converted into a transition energy through the relation of Eq. (7), which is also shown as the upper scale in Fig. 7. Two arrows in the figure represent the resonance positions in vacuum, 3.318 and 3.323 keV, for $J = 1/2$ and 3/2 states, respectively. The major feature of the fine structure is that the resonance splits into two dips, the lower transition energy dip further splits into two dips, the lowest transition energy dip has a wide tail to the lower energy side and the highest energy dip has a short tail to the higher energy side. These characteristics are well explained by the calculated transition energies shown in Fig. 2. Comparison between Figs. 7 and 2 indicates that the shape of the resonance curve is closely connected to the position dependence of the transition energies.

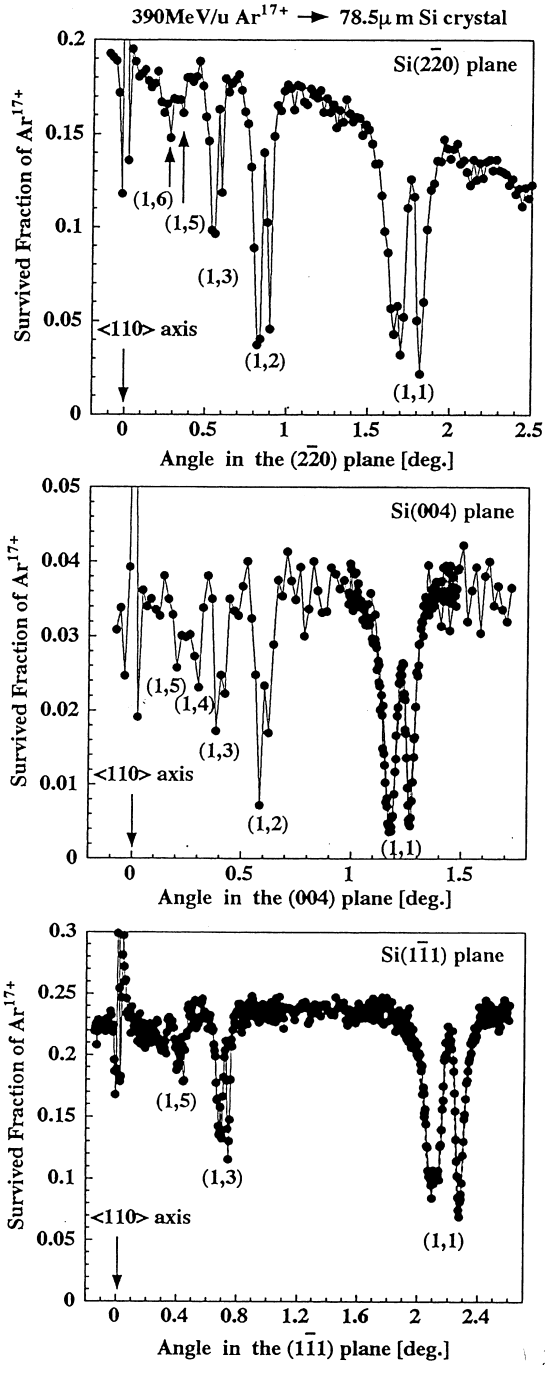

Fig. 6. Survived fraction of 390 MeV/u Ar^{17+} as function of angle between the ion velocity and the [1 1 0] axis along the (2 $\bar{2}$ 0), (0 0 4) and (1 $\bar{1}$ 1) planes.

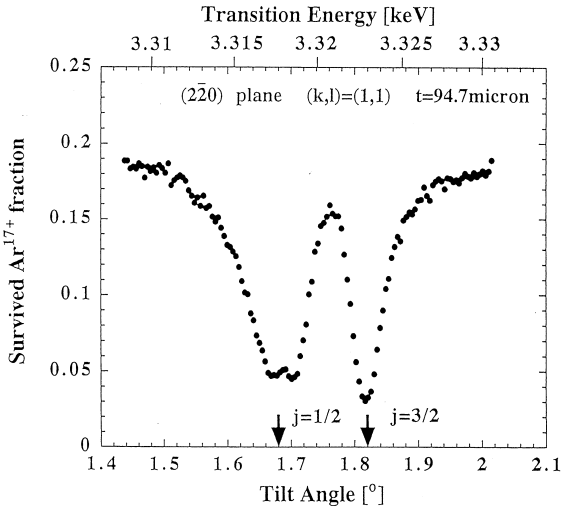

Fig. 7. Detailed angular scan of the (1,1) resonance for the (2 $\bar{2}$ 0) plane.

4.3. Correlation between resonance angle and the energy deposition

In the present, we simultaneously measured the energy deposited by the ion in the crystal, which we simply call 'energy loss'. Disregarding the difference in energy losses between Ar^{17+} and Ar^{18+}, which is considered to be at most 10%, i.e., $(18^2-17^2)/18^2$, the survived Ar^{17+} fraction, $f(\theta,\varepsilon)$, as a function of the tilt angle, θ, and the energy loss, ε, was re-histogrammed for the (1,1) resonance of the (2 $\bar{2}$ 0) plane.

As mentioned above, the tilt angle, θ, can be converted to the transition energy, ΔE. Furthermore, we converted the energy loss, ε, to the amplitude, A, of the ion trajectory by the help of a simulation [8]. Thus we get the survived fraction as a function of the transition energy and the trajectory amplitude, $f(\Delta E, A)$. The survived Ar^{17+} fraction, $f(A)$, from only 1s electron ionization is observed at the region of off-resonance condition. Then $F(\Delta E, A) = 1 - f(\Delta E, A)/f(A)$ can be regarded as the ionized fraction through RCE. Fig. 8 shows a contour map of $F(\Delta E, A)$ thus obtained. The calculated transition energies at the trajectory amplitude obtained from Fig. 2 are also shown in Fig. 8 by solid lines.

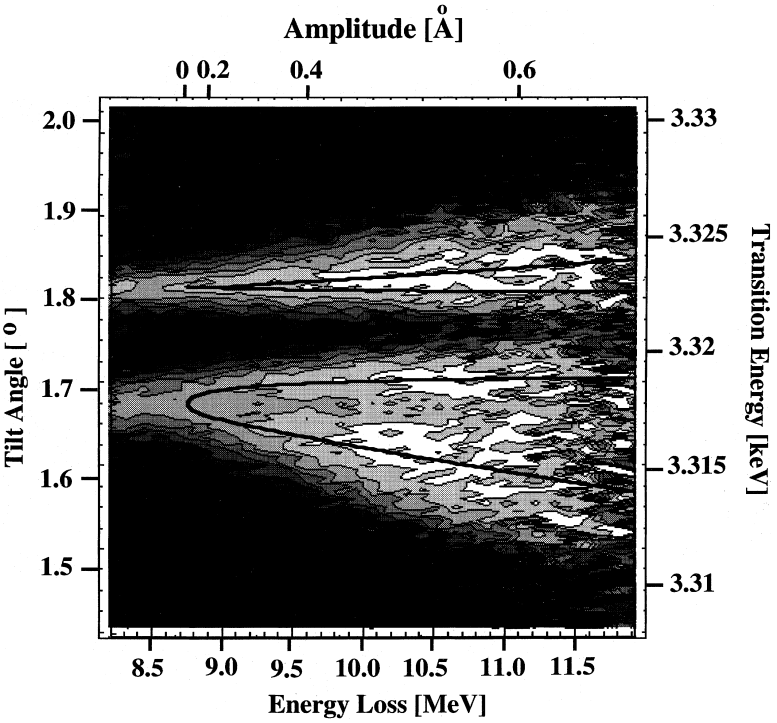

Fig. 8. Contour map of ionized fraction through resonant coherent excitation as a function of tilt angle (equivalent to transition energy) and energy deposition (equivalent to trajectory amplitude).

At the lowest energy deposition, the RCE probability shows two narrow peaks and as the trajectory amplitude increases, the higher transition energy RCE broadens without shifting and the lower transition energy RCE splits into two peaks. These features are excellently reproduced by the calculated lines. This means that the oscillatory ion trajectory with a finite amplitude results in various transition energies, which induces the broadening, however, the channeled ions spend the longer time at the maximum amplitude and the oscillating perturbation generally increases with distance from the channel center, thereby, the RCE process tends to take place at the largest amplitude of the trajectory.

Acknowledgements

This work was in part supported by a Grant-in-Aid for Scientific Research from the Ministry of Education, Science and Culture (07404019), and also by a research project with heavy ions at NIRS-HIMAC.

References

[1] V.V. Okorokov, Yad. Fiz. 2 (1965) 1009; Sov. J. Nucl. Phys. 2 (1966) 719.
[2] S. Datz, C.D. Moak, O.H. Crawford, H.F. Krause, P.F. Dittner, J. Gomez del Campo, J.A. Biggerstaff, P.D. Miller, P. Hvelplund, K. Knudsen, Phys. Rev. Lett. 40 (1978) 843.
[3] F. Fujimoto, K. Komaki, A. Ootuka, E. Vilalta, Y. Iwata, Y. Hirao, T. Hasegawa, M. Sekiguchi, A. Mizobuchi, T. Hattori, K. Kimura, Nucl. Instr. and Meth. B22 (1988) 354.
[4] H.F. Krause, S. Datz, Adv. Atomic, Mol. and Opti. Phys. 37 (1996) 139.
[5] T. Azuma, T. Ito, Y. Yamazaki, K. Komaki, M. Sano, M. Torikoshi, A. Kitagawa, E. Takada, T. Murakami, Nucl. Instr. and Meth. B, 135 (1998) 61.

[6] T. Ito, T. Azuma, K. Komaki, Y. Yamazaki, T. Murakami, E. Takada, A. Kitagawa, M. Torikoshi, M. Sano, Phys. Scripta T73 (1997) 345.
[7] T. Azuma, K. Komaki, Y. Yamazaki, N. Kakutani, S. Ninomiya, K. Maki, T. Takahira, M. Sekiguchi, T. Hattori, T. Hasegawa, Nucl. Instr. and Meth. B 115 (1996) 306.
[8] T. Ito, T. Azuma, K. Komaki, Y. Yamazaki, Nucl. Instr. and Meth. B, 135 (1998) 132.